Nanoscale

PAPER

View Article Online
View Journal | View Issue

Check for updates

Cite this: *Nanoscale*, 2017, **9**, 14730

Influence of surface coating on the intracellular behaviour of gold nanoparticles: a fluorescence correlation spectroscopy study†

A. Silvestri,‡[a,b] D. Di Silvio,‡[c] I. Llarena,[c] R. A. Murray,[c] M. Marelli,[a] L. Lay,[b,d] L. Polito *[a] and S. E. Moya *[c]

In the biomedical applications of nanoparticles (NPs), the proper choice of surface chemistry is a crucial aspect in their design. The nature of the coating can heavily impact the interaction of NPs with biomolecules, affect the state of aggregation, and ultimately determine their biological fate. As such, protein corona formation and the aggregation behaviour of gold NPs (Au NPs) are studied here. Au NPs are prepared with four distinct surface functionalisations, namely mercaptosuccinic acid (MSA), *N*-4-thiobutyroil glucosamine, HS-PEG_{5000} and HS-alkyl-PEG_{600}. Corona formation, aggregation, and the intracellular behaviour of the Au NPs are then investigated by means of Fluorescence Correlation Spectroscopy (FCS) in cell culture media and in live cells. To evaluate the state of aggregation and the formation of a protein corona, the Au NPs are incubated in cell media and the diffusion coefficient is determined *via* FCS. The *in vitro* behaviour is compared with the level of aggregation of the NPs in cells. Diffusion times of the NPs are estimated at different positions in the cell after a one hour incubation period. It is found that the majority of MSA and glucose-Au NPs are present inside the cell as slowly diffusing species with diffusion times (τ_D) greater than 6000 μs (hydrodynamic diameter >250 nm). PEGylated Au NPs adsorb a small amount of protein and manifest low agglomeration both in media and in living cells. In particular, the HS-alkyl-PEG_{600} coating shows an excellent correlation between lower protein adsorption, 4-fold lower compared to the MSA coated NPs, and limited intracellular aggregation. In the case of single HS-alkyl-PEG_{600} coated NPs, it is found that typical intracellular τ_D values range from 500 to 1500 μs, indicating that these particles display reduced aggregation in the intracellular environment.

Received 27th June 2017,
Accepted 1st September 2017

DOI: 10.1039/c7nr04640e

rsc.li/nanoscale

Published on 01 September 2017. Downloaded by CIC biomaGUNE on 10/10/2017 11:32:18.

Introduction

In biomedical applications, the surface coating of nanoparticles (NPs) is usually designed to minimise unspecific interactions, increase circulation, or to promote targeted delivery of the NPs to specific organs and cells, where they fulfil their therapeutic function. The biological fate, therapeutic efficacy, and toxicity of NPs are determined largely by their surface chemistry.[1–3]

In the biological environment, NPs interact with surrounding biomolecules, resulting in the formation of a corona around the NPs, which can confer a new "biological identity" to the NPs[4–6] This new interface should then determine the interaction of the NPs with other biomolecules or cells. Often, the formation of a corona causes NP aggregation, but it can also reduce aggregation by stabilizing single NPs, thereby either enhancing or reducing cell uptake,[7] and effectively influencing their biodistribution and intracellular trafficking.[8–10] Moreover, the aggregation of NPs *in vivo* is often not desired and may lead to an accumulation in the lungs[11] or their clearance by the mononuclear phagocyte system (MPS), thus preventing the NPs from reaching a specific organ. In biomedical applications, it is crucial to avoid the unspecific NP accumulation in undesired organs, maintaining a prolonged circulation time and efficient renal clearance.[12]

Surface functionalisation is a common strategy to increase the circulation time and minimise the unspecific cellular uptake of NPs. The surface coating may consist of molecules characterised by low protein affinity, thereby minimising protein corona formation and aggregation. Currently, several coatings are available, glycans, polyethylene glycol (PEG), zwitterionic surfactants, *etc.*, of which PEG is the most commonly

[a]*CNR – ISTM, Nanotechnology Lab., Via G. Fantoli 16/15, 20138 Milan, Italy. E-mail: laura.polito@istm.cnr.it*
[b]*Department of Chemistry, University of Milan, Via C. Golgi 19, 20133 Milan, Italy*
[c]*Soft Matter Nanotechnology Group, CIC biomaGUNE, Paseo Miramon, 182, 20009 San Sebastian, Spain. E-mail: smoya@cicbiomagune.es*
[d]*CRC Materiali Polimerici (LaMPo), University of Milan, Via C. Golgi 19, 20133 Milan, Italy*

†Electronic supplementary information (ESI) available. See DOI: 10.1039/c7nr04640e

‡These authors contributed equally to the article.

This journal is © The Royal Society of Chemistry 2017

Published on 01 September 2017. Downloaded by CIC biomaGUNE on 10/10/2017 11:32:18.

used for functionalisation. PEG is associated with a higher affinity to water but low or no net charge that inhibits protein binding.[13–16] For PEG, antifouling properties largely depend on PEG molecular weight and orientation on the surface. The orientation can be modified by placing a spacer between the NP surface and the PEG moiety. The proper choice of the PEG ligand is therefore fundamental for achieving an effective antifouling coating. Several studies have been performed on PEG, including the influence of its molecular characteristics, the orientation/arrangement on NPs, and its interaction with proteins.[7,17,18] However, little is known about its impact on the state of aggregation of NPs *in vitro* or in the intracellular environment.

An important issue in the design of a suitable antifouling coating is to understand to what extent the antifouling character provided by the coating is preserved upon NP uptake. Following uptake, NPs are often confined to acidic vacuoles with their trafficking in cells being affected by the interaction with the various biomolecules and cell components. All these interactions can affect the final NP surface composition, as well as the state of aggregation.[19,20]

Fluorescence Correlation Spectroscopy (FCS) is a technique based on recording fluorescence fluctuations in a confocal volume, related to the diffusion of the fluorescent molecules. Diffusion times can be correlated with the size of the diffusing species, and also with the local micro-environmental conditions, *i.e.* local viscosity and temperature.[21–23] In recent years, FCS has frequently been used to study the hydrodynamic size of NPs in different biological media[24–26] and to characterise the protein corona structure and composition.[27,28] In particular, by means of FCS, it is possible to characterise the NP-protein affinity constants,[29,30] the effect of different ligands on the protein corona formation[31,32] and the arrangement of some proteins around the NP surface.[33] Murray *et al.*[34] studied the intracellular dynamics of glucose functionalised Au NPs by means of FCS. In this study, we focused on the NP stability inside cell compartments and it was shown that glucose functionalised NPs were not only present in intracellular vesicles forming large aggregates, but were also found to be located in the cytosol as small homogeneous NPs with protein corona population or as small NP aggregates. Other approaches have also been followed to study the intracellular fate of NPs. It is worth mentioning the work of Bertoli and coworkers where using a combination of protein fluorescence labelling and cell organelle separation, the authors were able to highlight the changes in the protein corona on different NPs after cellular internalization and accumulation in lysosomes.[35] Another study combined the experimental observation of NP uptake with correlation statistical analysis to predict the effect of NP internalization on cellular organelle distribution inside cells.[36]

In the work presented here, we aim to study the influence of the molecular characteristics of different ligands on gold (Au) NPs *in vitro*, evaluating the state of aggregation *in vitro* and during intracellular trafficking. Our aim is to understand whether or not the properties, conferred by the ligands, are retained by the NPs following uptake. We hope that these findings will aid in the future design of more efficient, target specific intracellular probes. Here we present a study of NPs with four distinct surface coatings, namely: (1) a long chain PEG (MW 5 kDa), PEG_{5000}; (2) an amphiphilic polymer composed of a short PEG (MW 600 Da) and an alkyl chain, alkyl-PEG_{600}; (3) mercaptosuccinic acid; (4) *N*-4-thiobutyroil glucosamine. The two low molecular weight ligands are widely used as stabilising agents in aqueous solutions. *In vivo*, they confer a certain ability to reduce NP clearance by macrophages.[37–39] PEG_{5000} is widely used as an antifouling agent for NPs and surfaces,[40] while alkyl-PEG_{600} is interesting due to the simultaneous presence of a hydrophilic and an aliphatic chain which yields tighter ligand packing.[41] NP protein corona formation and aggregation in several media and stability as a function of time were studied by FCS, using properly labelled NPs. *In vitro*, FCS results were validated by transmission electron microscopy (TEM), dynamic light scattering (DLS) and UV-vis spectroscopy. Finally, NP internalisation was tracked by FCS and confocal laser scanning microscopy (CLSM). Finally, four regions of interest were identified in the cells, within which FCS was employed to estimate the state of aggregation and the effect of the choice of ligand.

Results and discussion

In vitro characterisation of NPs

Au NPs are widely employed in biomedical applications due to their high degree of biocompatibility. Au can form stable bonds with sulfur, thereby offering multiple possibilities for functionalisation which open various avenues for imaging, targeting, and modifying NPs *via* the use of thiols. In this work, Au NPs were produced according to a reported "one-pot" synthesis which allows good control over the size and shape.[42] Four different molecules were selected to functionalise the Au NP surface (see Fig. 1): mercaptosuccinic acid, *N*-4-thiobutyroil glucosamine, HS-PEG_{5000}, and an amphiphilic HS-alkyl-PEG_{600} chain. Additionally, a fluorescent dye was attached to the NP surface to facilitate fluorescence studies (see Fig. 2a). A detailed description of all ligands and Au NP synthetic procedures is included in the ESI (sections S1–S3†). NPs were

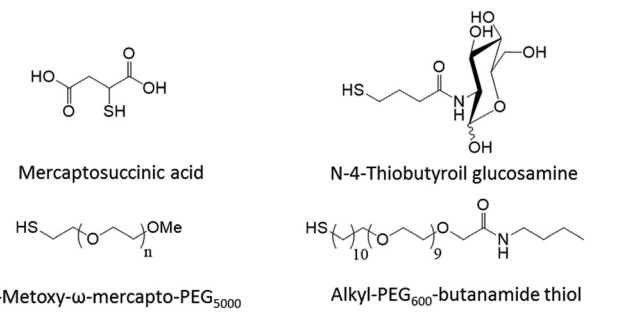

Fig. 1 Chemical structures of the ligands selected for the coating of Au NPs.

Published on 01 September 2017. Downloaded by CIC biomaGUNE on 10/10/2017 11:32:18.

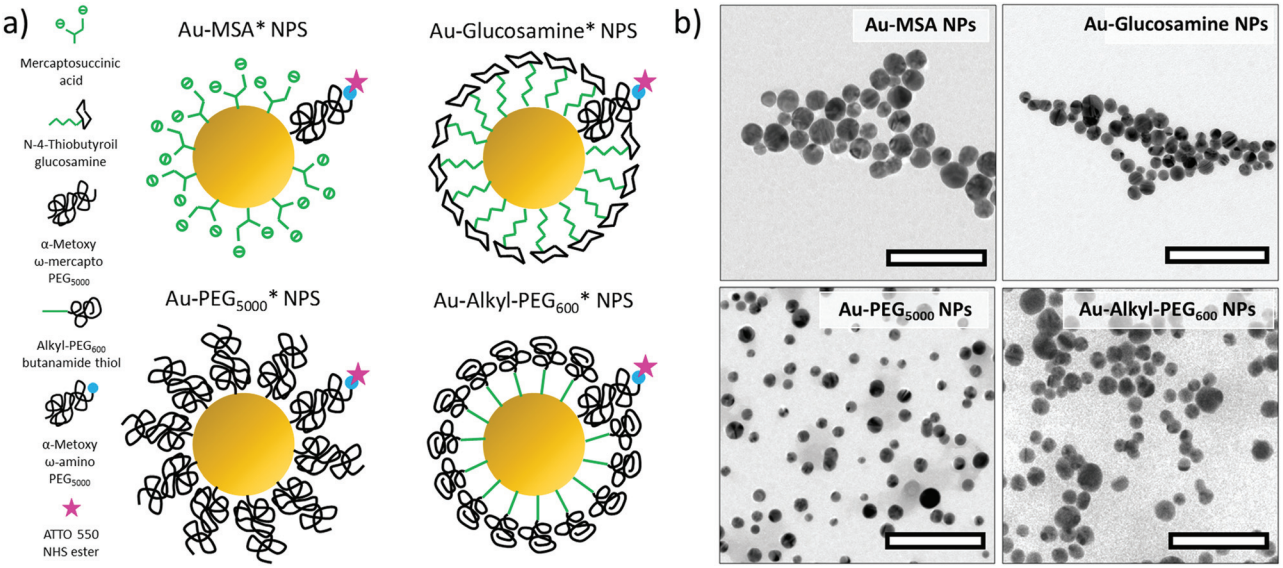

Fig. 2 (a) Sketch of the designed Au NPs employed in the study and (b) related TEM micrographs of the Au NPs. The scale bar is 100 nm.

characterised by means of Transmission Electron Microscopy (TEM), UV-vis spectroscopy, and Dynamic Light Scattering (DLS). TEM showed that Au NPs range in diameter from approximately 14 to 22 nm (Fig. 2b). ATTO550 was chosen as a fluorescent molecule, being characterised by a strong absorption, high fluorescence quantum yield, and high thermal and photo-stability. HS-PEG_{5000}-NH_2 was introduced on the NP coating to covalently link ATTO550 and, as the dye is moderately hydrophilic and adds a positive charge to the coupled molecule, only 10% of the total ligand amount was substituted by amino-PEG (Fig. S9–S12†). In the following discussion, NPs will be distinguished into non-fluorescent NPs: Au-MSA NPs, Au-glucosamine NPs, Au-alkyl-PEG_{600} NPs, and Au-PEG_{5000} NPs; and fluorescent labelled NPs: Au-MSA* NPs, Au-glucosamine* NPs, Au-alkyl-PEG_{600}* NPs, and Au-PEG_{5000}* NPs.

Tables S5–S7† show the hydrodynamic diameters of the AU NPs, for each of the four surface modifications used, as determined by three separate methods: FCS, DLS and UV-vis spectroscopy (this reveals that the particle with the largest diameter is seen to be Au PEG_{5000}, while the glucosamine Au NPs are seen to have the smallest diameter). This stands to reason as the long hydrophilic PEG chains become extended in aqueous solution. In the case of glucosamine, it is likely that the ligand density is sufficiently low that it remains relatively unextended. The two other surface coatings showed relatively similar hydrodynamic diameters of 8 and 9 nm.

RPMI 1640 and full RPMI 1640 enriched with 10% fetal bovine serum (FBS) are commonly used media for cell culture. When NPs are exposed to these media, NP aggregation and the formation of a protein corona usually occur.[43] These events affect the cellular uptake of NPs and highlight the need to better understand and characterise NPs in such environments. FCS is particularly powerful in this regard because of the possibility to perform experiments *in situ*.

Fig. 3 shows FCS data with different correlation functions for the free dye, proteins and NPs. From the correlation functions, we are able to discriminate even the variation in the hydrodynamic diameter of Au NPs HD in the presence of FBS proteins.

In Fig. 4a, we report the hydrodynamic diameters of NPs dispersed in water, RPMI, and full RPMI as estimated by FCS. Given the dynamic nature of the protein corona formation, we followed its evolution in a time window of one hour.[3,9,37,44] We chose to operate in this time window as it has been described as the most dynamic, where the majority of the protein–NP interactions take place. Au-MSA* NPs and Au-glucosamine* NPs showed a significant increase in hydrodynamic diameter (>20 nm) in RPMI compared to water (Fig. 4a). This effect can be ascribed to a charge shield due to the high ionic strength of the media and to the presence of small molecules (*i.e.* lipids, sucrose), which can induce NP aggregation. Moreover, the high standard deviation suggests the formation of aggregates with heterogeneous dimensions. The effect of the medium observed on Au-alkyl-PEG_{600}* NPs and Au-PEG_{5000}* NPs was almost negligible, excluding NP aggregation and suggesting a modification of the hydrodynamic shells caused by salts and small molecules present in the medium.

When the FBS solution is added to the NPs in RPMI (full RPMI), a reduction in hydrodynamic diameter is observed. The addition of proteins by simple pipette mixing seems to promote disassembling of NP aggregates in favour of smaller, more stable NP–protein complexes. The effect is appreciable after just 5 minutes of incubation, in accordance with previously reported observations in the literature.[9] This results primarily as a consequence of the electrostatic and steric stabilization of the NPs being enhanced by protein adsorption.[43] Once formed, the evolution of the protein corona was followed over time. Changes in the corona are shown as variation in the diffusion time of the NPs and derived hydrodynamic diameters.

This journal is © The Royal Society of Chemistry 2017

Published on 01 September 2017. Downloaded by CIC biomaGUNE on 10/10/2017 11:32:18.

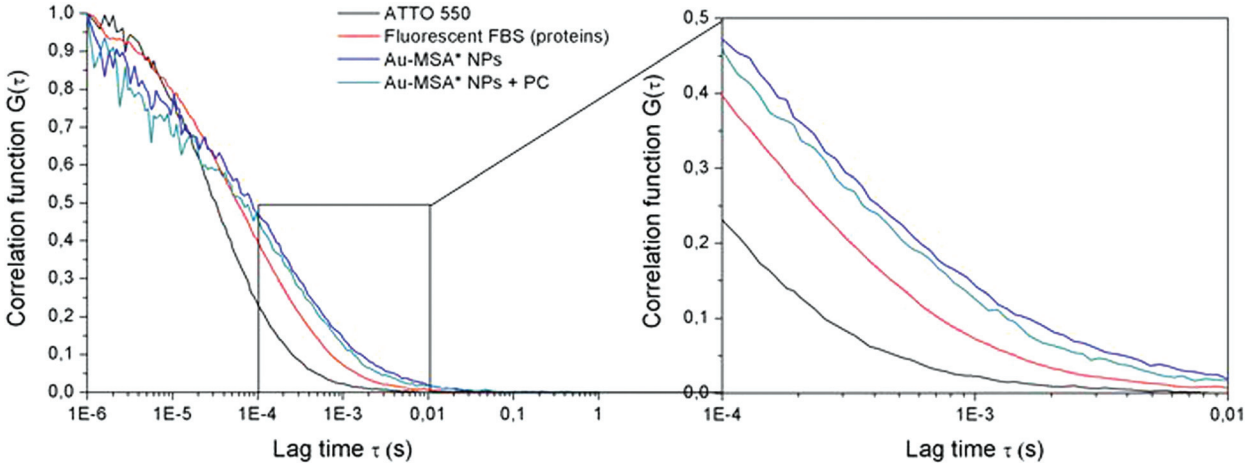

Fig. 3 Normalized correlograms of several species obtained by FCS. The black line refers to the free dye, the red line represents a mixture of FBS and dye, and the blue line and the green line represent Au-MSA* NPs before and after the formation of a protein corona, respectively. In the inset it is possible to better weigh the shift to higher lag times correlated with the increasing of the decay times of the species.

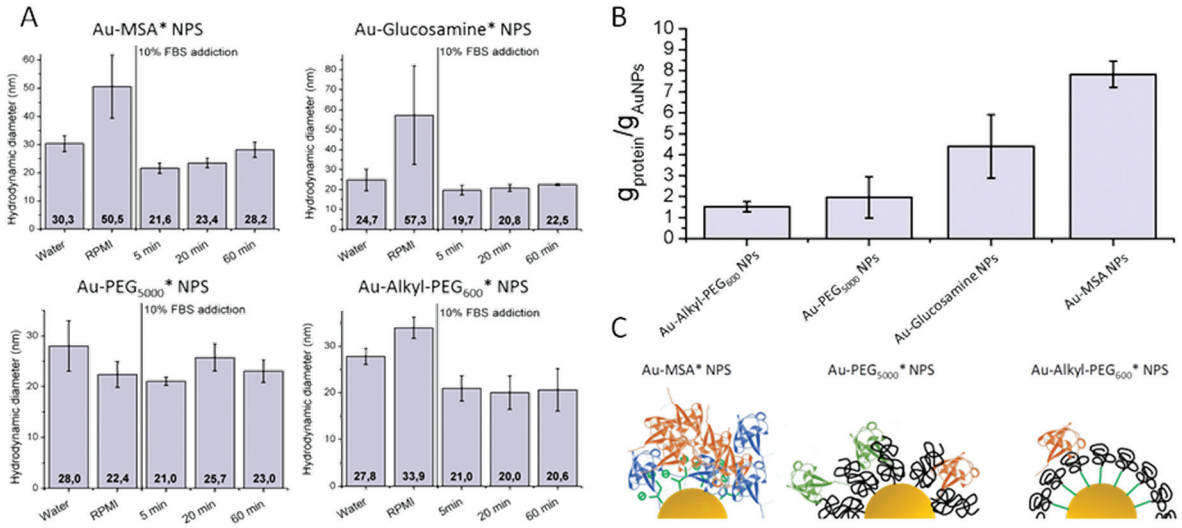

Fig. 4 Characterization of NPs in complex media. (a) Hydrodynamic diameter of the Au NPs * in water, RPMI and full RPMI (enriched with 10% of FBS) at 5, 20 and 60 min of incubation time. The data were derived from 3D fitting of the FCS correlograms and applying the Stokes–Einstein equation as described in the ESI.† (b) Colorimetric quantification of the proteins adsorbed on the Au NPs surface by the Pierce™660 protein assay. All the experiments were conducted in triplicates. (c) Scheme illustrating the proposed PC conformation for MSA, PEG_{5000} and alkyl-PEG_{600}-Au NPs. *p-Value <0.05.

After this initial screening process, the Au NPs were then incubated with FBS, and the hydrodynamic diameters were remeasured, in order to observe possible protein corona formation. Au-MSA* NPs were observed to increase in diameter by approximately 7 nm following a 1 hour incubation period (p-value <0.05). This may be attributed to protein corona formation, however it cannot be confirmed. The increase in diameter observed for Au-glucosamine* NPs is not significant and can be explained by the formation of either an incomplete protein corona or, more probably, a corona with a different composition and protein arrangement. The same could be applied to Au-PEG_{5000}* NPs whose data are in good agreement with the studies recently performed by Pelaz *et al.*[32] which reported a very limited final increase in hydrodynamic diameter for FePt NPs coated with a shell of poly(maleic anhydride-*alt*-dodecene) and PEG_{5000}. The authors reasoned that this small increment can be explained by the presence of a few protein molecules bound to PEGylated NPs or by the fact that proteins can partially penetrate into the PEG layers coating the NPs. Au-alkyl-PEG_{600}* NPs did not show significant changes in their hydrodynamic ratio in the presence of proteins over the observation time. This finding suggests that the chosen ligands, and the amphiphilic PEG in particular, are suitable for limiting the interaction between the proteins and the Au

Published on 01 September 2017. Downloaded by CIC biomaGUNE on 10/10/2017 11:32:18.

NPs while also minimising protein corona formation. In order to quantify the total protein concentration in the protein corona, a Pierce™ 660 Protein Assay was used. The results obtained are in close agreement with the latter observation and highlight the difference in the abundance of protein associated with the two PEGylated NPs (Fig. 4b). The amount of protein associated with Au-PEG_{5000} NPs was calculated to be 4-fold lower when compared to MSA* NPs (1.5–2 g_{prot}/g_{NP} *versus* 8 g_{prot}/g_{NP}). DLS (Fig. S13†) and UV-vis measurements (Fig. S14 and S15†) also indicate that alkyl-PEG_{600} inhibits protein complexation with the NP surface. Therefore, as extensively reported in the literature, it is reasonable to assume that a protein corona covering Au-MSA and glucosamine NPs is formed with this corona consisting of a layer of proteins absorbed on the NP surface with different affinities.[32] In contrast, Au-PEG_{5000} NPs might present an incomplete corona or a partial penetration of proteins into the PEG coating, while the alkyl portion introduced in the shell of the Au-alkyl-PEG_{600} NPs would hinder such a kind of interaction, resulting in the formation of an incomplete or less defined corona (Fig. 4c).

Intracellular dynamics of Au NPs

A549 cells were incubated with labelled Au NPs at a concentration of 15 μg ml^{-1}. FCS experiments were conducted after 30 min and one hour of incubation (Fig. 5a). The concentration of NPs applied for cell experiments was chosen as a compromise, on one hand, to perform fluorescence imaging, and on the other hand have a not too high fluorescence intensity that would difficult FCS measurements. Measurements were performed in living cells with the laser power being kept at a level such as to minimise photo-damage to cells. Confocal fluorescence microscopy images allow for the comparison of NP uptake at different time points. Cells treated with Au-MSA* and Au-glucosamine* NPs display increased uptake following a one hour incubation period. This is more evident in the case of Au-MSA* NPs. In contrast, both PEGylated NPs display lower uptake with respect to the non-PEGylated NPs. Following this observation, four regions were identified for further investigation of intracellular NP diffusion, namely the cytosol (CYT), the endoplasmic reticulum (ER), bright spots located close to the cell membrane (BS1), and bright spots surrounding the nucleus (BS2) (Fig. 5b). FCS experiments performed on the cellular membrane and nucleus show poor or no auto-correlation signals with diffusion times associated with proteins (τ_D < 500 μs) rather than NPs which do not accumulate in these compartments (Fig. S16†). The first two tracks that usually showed bleaching (due to the initial excitation) and the tracks showing low signal and visible aggregates were excluded from the analysis (Fig. S17†). Moreover, a negative control was used incubating free ATTO550 with the A549 cells. In this case, the same data analysis procedure used with Au NPs has been applied for demonstrating a different distribution of intracellular diffusing species (Fig. S18 and Tables S8, S9†).

Fig. 6 shows 4 representative auto-correlation curves for Au-MSA* NPs (one for each region of interest) fitted with a 3D normal diffusion fitting model with two diffusing components. This model, which provides good fits, allowed the description of the species in the confocal volume grouping them into two main populations that, despite being a simplification, helps to appreciate the system complexity.

The different positions inside the cells where the auto-correlation curves were recorded are shown in Fig. 6. The tracks were fit by a two component equation that allows an estimation of the fractional contribution of each component to the total collected signal. We report the component that gave the largest contribution (fraction percentage $\rho > 0.5$). For a detailed description of the statistical analysis of the tracks recorded, see the ESI (Fig. S18 and S19†).

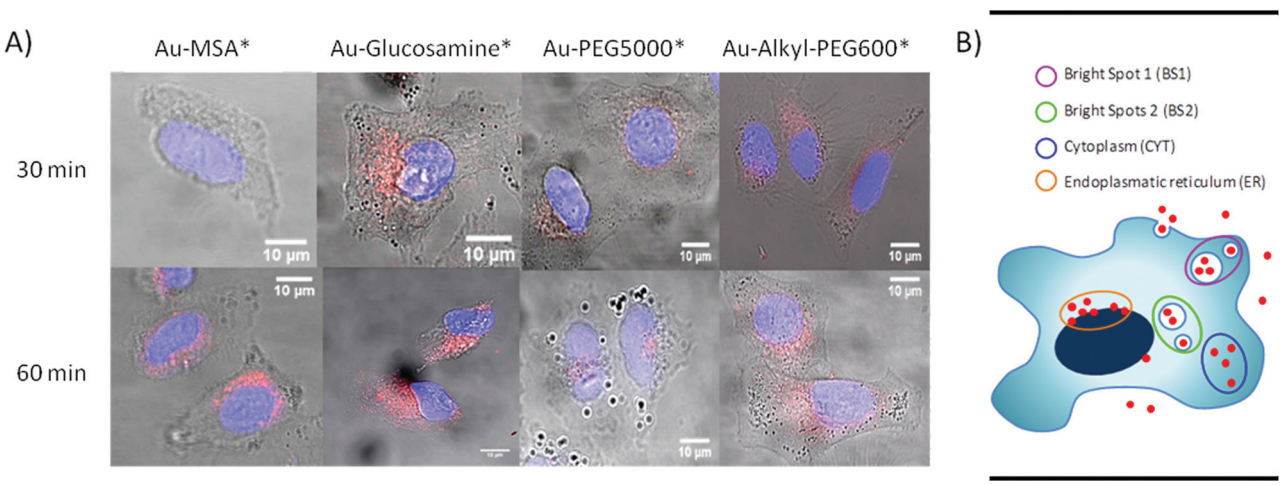

Fig. 5 (a) Confocal micrographs collected after 30 min and 1 hour of incubation. Nuclei were stained with Hoechst, NPs were labelled with ATTO550, cells were imaged in transmission mode. Excitation laser wavelengths were respectively 405 nm and 561 nm. Objective was 63× oil immersion lens (1.4 NA). (b) Schematic representation of the proposed NPs internalization pathway and of the regions of interest for the statistical FCS analysis.

 This journal is © The Royal Society of Chemistry 2017

Published on 01 September 2017. Downloaded by CIC biomaGUNE on 10/10/2017 11:32:18.

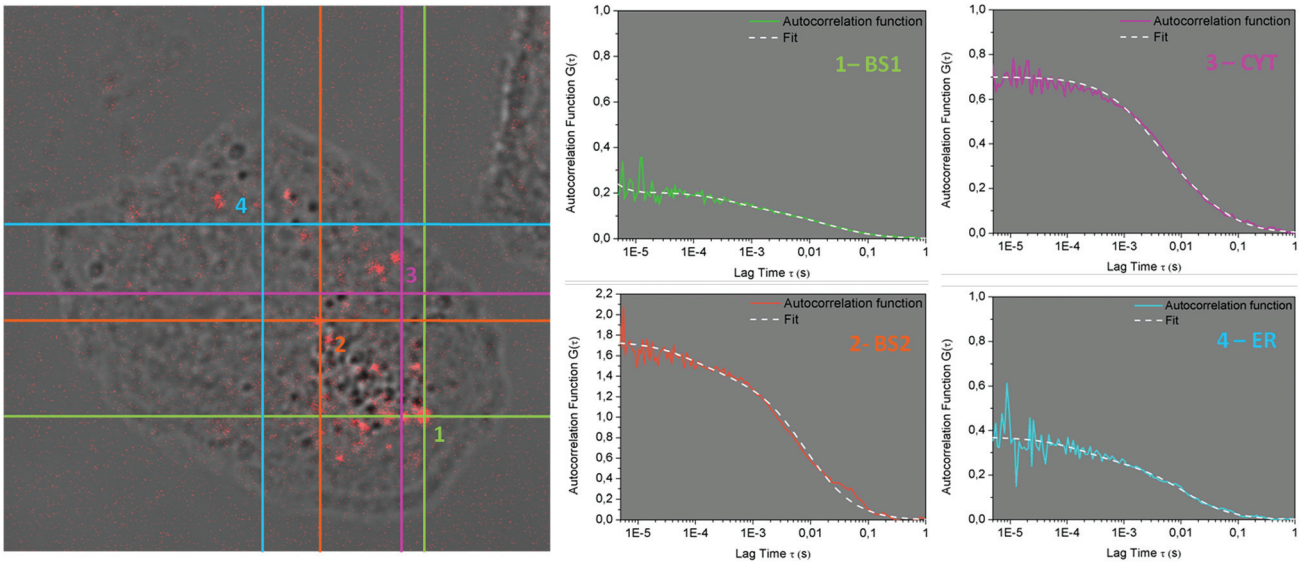

Fig. 6 (a) Confocal micrographs collected after 30 min and 1 hour incubation. Nuclei were stained by Hoechst, NPs were labelled by ATTO550, and the cells were imaged in transmission mode. Excitation laser wavelengths were 405 nm and 561 nm, respectively. The objective was 63× oil immersion lens (1.4 NA). (b) Schematic representation of the proposed NP internalization pathway and of the regions of interest for the statistical FCS analysis.

The fluorescent species in the confocal volume were characterised according to their diffusion time. They were grouped into four classes that were associated with different diffusing species: (i) 500 < τ_D (μs) < 1500: diffusion times of isolated free diffusing NPs; (ii) 1500 < τ_D (μs) < 3000: small aggregates of few NPs and/or NPs interacting with bio-macromolecules; (iii) 3000 < τ_D (μs) < 6000: aggregates of NPs; (iv) τ_D (μs) > 6000: large aggregates of NPs and/or NPs associated with cellular compartments. In Fig. 7, we can see the FCS autocorrelation curves that correspond to an incubation period of 30 minutes for NPs in the distinct cellular regions/compartments. As can be seen in the histograms, NPs coated with glucosamine were found in all compartments of the cell mostly as slowly diffusing species (red bars), with faster diffusing species found in the bright spots closer to the membrane (BS1) (green, yellow and orange bars), which reasonably might be associated with the recently taken up material. The other NPs are distributed inside the cells forming structures that are more heterogeneous. It is worth noting that in the case of Au-alkyl-PEG$_{600}$ NPs, species with diffusion times below 1500 μs (comparable to single diffusing NPs) have been detected in three compartments out of four (BS1, BS2, and ER). We ascribe this result to the higher stabilising effect of the ligand, which is capable of partially inhibiting or slowing down NP aggregation and/or association with cell compartments.

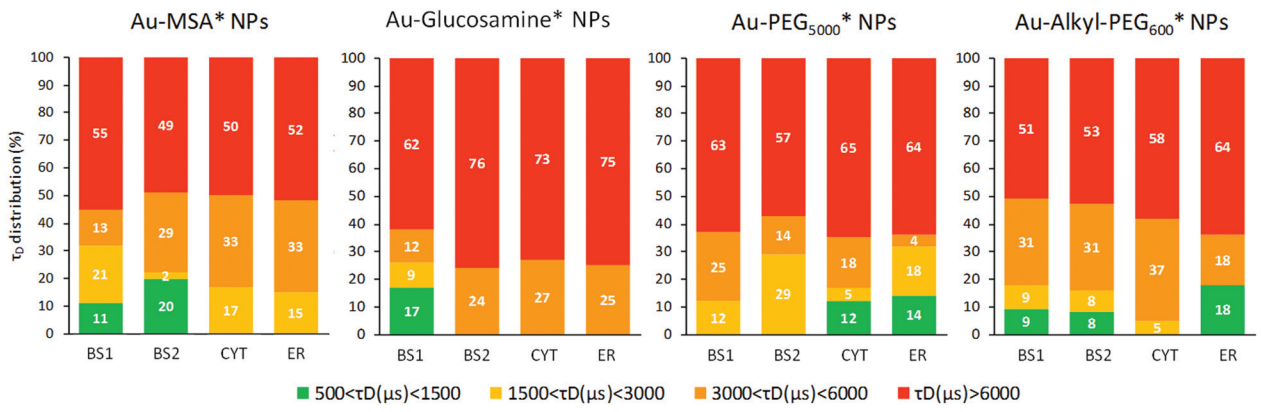

Fig. 7 Statistical analysis of the diffusion times recorded for different NPs inside A549 cells for 30 min. Percentage distribution of the decay times in the different regions of interest, grouped in four classes of diffusion times (500 < τ_D (μs) < 1500; 1500 < τ_D (μs) < 3000; 3000 < τ_D (μs) < 6000 and τ_D (μs) > 6000). Each section reports the results for Au-MSA* NPs, Au-glucosamine* NPs, Au-PEG5000* NPs and Au-alkyl-PEG$_{600}$* NPs. Bright spots 1 (BS1); bright spots 2 (BS2); ER = endoplasmic reticulum; CYT = cytoplasm.

Published on 01 September 2017. Downloaded by CIC biomaGUNE on 10/10/2017 11:32:18.

The difference between PEGylated and non-PEGylated NPs becomes more evident after one hour of incubation. We observe a significant shift towards a slowly diffusing species in all compartments of the cells treated with Au-MSA* and Au-glucosamine* NPs (Fig. S19†). This behaviour is remarkable in the bright spots where either single NPs are confined in a small space enriched with biomolecules (cellular vesicles) or are present as aggregates (Fig. 8a and b).

The data referring to bright spots close to the membrane (BS1) suggest the possible changes in the uptake pathways over time. We can speculate that after one hour of incubation, the protein corona formed around NPs increases in size, as discussed previously, and the accumulation of NPs on the membrane would bring NP uptake in the shape of visible aggregates >250 nm,[45] the resolution limit of the CLSM, with diffusion times >6000 μs. Our assumptions are in agreement with that extensively reported in the literature regarding similar NPs following uptake through different pathways,[46–48] as a result of the size of the species that is one of its main determinants (Fig. S21 and S22†). In the case of Au-MSA* NPs, at first, they show a wide distribution of diffusing species in all compartments, comparable to the PEGylated NPs: 45% of the analysed tracks expressed diffusion times below 6000 μs in BS1, 51% in BS2, 50% in the cytoplasm and 48% in the endoplasmic reticulum. As shown in Fig. 5a, we observed similarities in the aggregation behaviour after 30 min of incubation among MSA*, PEG_{5000}* and alkyl-PEG_{600}* NPs, as they showed a lower amount of agglomeration compared to Au-glucosamine* NPs. The intracellular behaviour of Au-MSA* NPs, following one hour of incubation, was observed to be more similar to that of Au-glucosamine* NPs. This is typified by high uptake and the presence of large bright spots, identified in confocal images as aggregates, indicative of limited intracellular colloidal stability. They were mainly detected as species with diffusion times greater than 6000 μs in BS1 (90% of the tracks), in BS2 (100%) and in the cytoplasm (79%). In contrast, the distribution of diffusion times of Au-PEG_{5000} and Au-alkyl-PEG_{600}* NPs was unchanged; instead they expressed an overall higher colloidal stability both in media and in cell compartments. We assume that PEGylated NPs are taken up partially through the formation of vesicles, seen as bright spots in the confocal images. Looking at BS2, it is also possible to distinguish different behaviours between Au-PEG_{5000}* and Au-alkyl-PEG_{600}* NPs. In fact, for Au-PEG_{5000}* NPs, after 1 hour of incubation, all the fluorescent species were found to display diffusion times greater than 3000 μs. In contrast, for Au-alkyl-PEG_{600}* NPs, there were still populations with diffusion times in the range of $500 < \tau_D(\mu s) < 3000$, 26% of the tracks below 3000 μs and 51% < 6000 μs, indicating the presence of single free diffusing nanoparticles or small aggregates. Moreover, the changes in diffusion time values and percentage distributions are minimal (Fig. S20†).

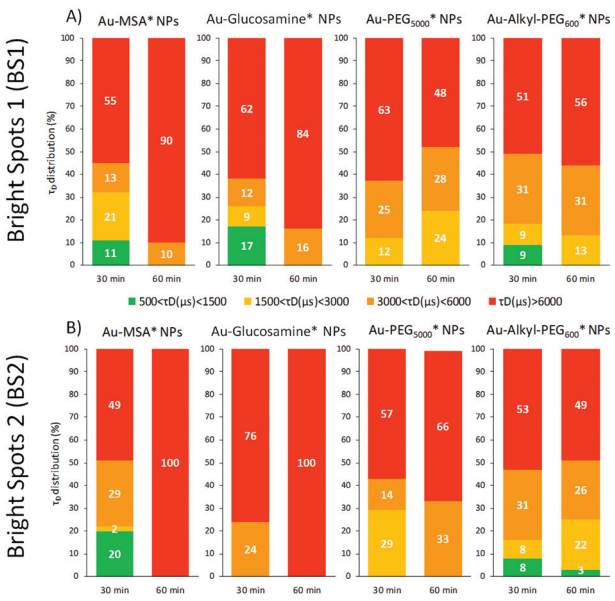

Fig. 8 Percentage distribution of the main diffusing species obtained from fitting tracks ($n > 30$) by a 3D normal diffusion model. The diffusion times were grouped in four classes ($500 < \tau_D$ (μs) < 1500; $1500 < \tau_D$ (μs) < 3000; $3000 < \tau_D$ (μs) < 6000 and τ_D (μs) > 6000). Results for Au-MSA* NPs, Au-glucose* NPs, Au-PEG_{5000}* NPs and Au-alkyl-PEG_{600}* are reported at 30 and 60 minutes of incubation. (a) Bright spots 1 (BS1); (b) bright spots 2 (BS2).

Conclusions

In summary, the intracellular dynamics of the NPs seems to reflect the properties of the coatings observed *in vitro*. In full RPMI, glucosamine and MPS functionalized Au NPs presented a strong affinity toward proteins; however, once internalised in cells, they showed reduced stability and more prominent formation of aggregates and complexes with cellular macromolecules. In contrast, PEGylated NPs, and in particular alkyl-PEG_{600} Au NPs, which display a lower affinity toward proteins, show a reduced propensity to form aggregates intracellularly with greater stability. This means that from a practical point of view, the engineering of the NPs with molecules like PEG to avoid or decrease the interaction with proteins is also effective in decreasing NP aggregation in the cell, which can impact NP translocation and has consequences in their applications for targeted drug delivery.

Experimental

Materials and methods

$HAuCl_4 \cdot 3H_2O$, $AgNO_3$, hydroquinone, 4,4′-dithiodibutyric acid, glucosamine hydrochloride, butylamine, 1-ethyl-3-(3-dimethylaminopropyl)carbodiimide (EDC), *N*,*N*′-dicyclohexylcarbodiimide (DCC), *N*-hydroxysuccinimide (NHS), 1,4-dithiothreitol (DTT) and NaOH were purchased from Sigma-Aldrich, and used without further purification. $HAuCl_4 \cdot 3H_2O$ was stored at 4 °C, shielded from light, as 10 mM solution, and NaOH was stored as 1 M water solution. 10 mM $AgNO_3$ and

This journal is © The Royal Society of Chemistry 2017

Published on 01 September 2017. Downloaded by CIC biomaGUNE on 10/10/2017 11:32:18.

hydroquinone solutions were freshly prepared before each synthesis (avoiding exposure to light). HS-PEG_{5000}-OCH_3 and HS-PEG_{5000}-NH_2, purchased from Rapp Polymere GmbH, were used as received and stored under a dry argon atmosphere at −20 °C. HS-alkyl-PEG_{600}-COOH (([1-mercaptoundec-11-yl] PEG_{600})-acetic acid) was synthesised by Chorisis srl. (Varese, Italy) following a literature reported procedure.[41] A549 cells (human lung cancer) were purchased from ATCC. The cells were cultured in RPMI 1640 medium from Lonza, and supplemented with 10% fetal bovine serum (FBS) and 1% penicillin–streptomycin from Sigma Aldrich.

The Au NPs were synthesised employing a 'one-pot' strategy described by Silvestri *et al.*[42] The selected ligands were added directly to the reaction mixture to stop the growth and cap the NPs. In this way, a panel of four Au NPs characterised by different coatings were made. For all NPs, 10% of the surface was coated introducing a α-amino-ω-thiol PEG_{5000} to allow the subsequent labelling of the system with ATTO550 fluorescent dye (ATTO-TECH GmbH). We selected a long amino PEG chain in order to have a large distance between the metallic core and the fluorophore molecule, reducing the quenching effect due to the presence of the noble metal. We choose to cover 10% of the surface with α-amino-ω-thiol PEG_{5000} to have a good fluorescence signal with a slight modification of the NP surface.

NPs were characterised extensively by TEM, UV-vis spectroscopy, DLS, and fluorescence correlation spectroscopy (FCS) in media and in live cells. Proteins present in the corona were quantified by Pierce™ 660 Protein Assay. The cells were imaged by CLSM. For detailed procedures, see the ESI.†

FCS experiments in water. Stock solutions of ATTO 550 labelled Au NPs with a concentration of 1 mg ml^{-1} were prepared. Prior to each FCS measurement, the solutions were sonicated for 5 min and double filtered on 0.22 μm regenerated cellulose syringe filters. This operation helps to remove the excess of free fluorophore that can remain electrostatically attached to the surface of the Au NPs. To perform the FCS measurements, 25 μl of Au NPs were dissolved in 225 μl of MilliQ water. Each sample of NPs was measured in 3 independent experiments, each comprising 10 runs of 10 seconds. For each measurement session, 50 nM water solutions of rhodamine B and of ATTO 550 were measured to determine the structural parameter and the diffusion coefficient of the free dye. Before performing the measurements, the ConfoCor and FCS x–y alignment was checked following the procedure of Altan-Bonnet[49] (Fig. S23†). The excitation wavelength was 561 nm and the objective was 40× water immersion.

FCS experiments in full RPMI cellular medium. Stock solutions of ATTO 550 labelled Au NPs with a concentration of 1 mg ml^{-1} were prepared. Prior to each FCS measurement, the solutions were sonicated for 5 min and double filtered on 0.22 μm regenerate cellulose syringe filters. This operation helps to remove the excess of free fluorophore that can remain electrostatically attached to the surface of the Au NPs. To perform the FCS measurements, 25 μl of Au NPs were dissolved in 225 μl of a phenol red free RPMI solution, enriched with 10% in volume of FBS. The FCS measurements were recorded at 10 min, 20 min, and 1 h after the mixing of the solutions. Each NP sample was measured in 3 independent experiments, each comprising 10 runs of 10 seconds. In comparison, a FCS measurement was performed on bare NPs in RPMI. For each measurement session, 50 nM water solutions of rhodamine B and of ATTO 550 were measured to determine the structural parameter and the diffusion coefficient of the free dye. The diffusion coefficient of proteins was determined mixing 25 μg of FBS with a 50 nM solution ATTO 550 in RPMI. FCS measurements were performed as in water.

FCS experiments in living cell. A549 cells were grown in RPMI media enriched with 10% of fetal bovine serum (FBS) and 1% of penicillin–streptomycin (PS) under a humidified atmosphere at 37 °C with 5% CO_2. To perform FCS on live cells, 10 000 A549 cells were seeded on NuncTM Lab-Tek Chambered Coverglass (purchased from Thermo Fisher Scientific) and grown under a humidified atmosphere at 37 °C with 5% CO_2 for 24 hours. The cells were incubated with 500 μl of 15 μg ml^{-1} solution of fluorescently labelled Au NPs for 30 and 60 minutes. The cells were washed twice with warm PBS. To perform the experiments in living cells, these were kept in 10 mM of Hepes. The microscope objective used for FCS on live cells was a 40× water immersion objective. The excitation wavelength was 561 nm and the cells were imaged in transmission mode. FCS measurements were performed on at least 3 cells recording 20 runs of 10 seconds each in 8 distinct areas inside the cell: 2 in the cytoplasm (CYT); 2 in the endoplasmic reticulum (ER) and, whenever visible, 2 in brighter spots near to the membrane (bright spots 1, BS1) and 2 in brighter spots near to the nucleus (bright spots 2, BS2). Moreover, one experiment was performed on/close to the membrane and one on/close the nucleus.

CLSM imaging of cells. For imaging, cells were washed with PBS and the endoplasmic reticulum was stained with ER-Tracker Green (BODIPY FL glibenclamide) (Invitrogen, E34251) over 10 min at 37 °C. Two more washes were performed and the cells were fixed with 3.7% paraformaldehyde (2 min at 37 °C). After washing again, the nuclei were stained with Hoechst 33342 Solution (20 mM) (Thermo Fisher Scientific) for 5 min at r.t. The cells were finally washed and kept in PBS. The stained cells were examined under a laser scanning confocal microscope (LSM 510 Meta confocal microscope Zeiss, Germany) equipped with a 63× oil objective lens (1.4 NA). Images were acquired sequentially to avoid cross-talk using excitation wavelengths 405, 488 and 561 for Hoechst, ER staining and ATTO550, respectively. Processing and overlay with transmission images were performed with Image J free software.

Protein quantification assay. Proteins composing the corona were quantified by the Pierce™ 660 Protein Assay (Thermo Scientific). The protein's calibration curve was obtained by measuring BSA standard solutions ranging from 25 μg ml^{-1} to 1000 μg ml^{-1}. 100 μl of protein solution was incubated with 1.5 ml of Pierce TM 660 Protein Assay Reagent for 1 h. The absorption spectra of the samples were recorded by employing a mixture of 100 μl of PBS and 1.5 ml of Pierce™ 660 Protein

Published on 01 September 2017. Downloaded by CIC biomaGUNE on 10/10/2017 11:32:18.

Assay Reagent as a baseline. The absorbance values at 660 nm were taken into account to build the calibration curve.

For the quantification of the PC proteins, 915 μg of NPs were incubated overnight in 1 ml of pure FBS at 37 °C. The PC NPs were separated from the excess of proteins employing centrifugation (15 000 rpm for 1 h) over a layer of 0.7 M sucrose (700 μl). The supernatant was removed and a pellet of NPs was isolated. Each pellet was suspended in 100 μl of PBS and 1.5 ml of Pierce™ 660 Protein Assay Reagent was added and incubated for 1 h. The absorbance at 660 nm was recorded on diluted samples in triplicate. The spectra of bare Au NPs were recorded to subtract the absorbance contribution at 660 nm.

Conflicts of interest

There are no conflicts to declare.

Acknowledgements

D. Di Silvio, I. Llarena and S. Moya acknowledge the ERA-NET SIINN FATENANO for support. L. Polito and L. Lay acknowledge MIUR-Italy (contract 2015RNWJAM_002) for financial support.

Notes and references

1 M. J. D. Clift, B. Rothen-Rutishauser, D. M. Brown, R. Duffin, K. Donaldson, L. Proudfoot, K. Guy and V. Stone, *Toxicol. Appl. Pharmacol.*, 2008, **232**, 418–427.
2 A. Banerjee, J. Qi, R. Gogoi, J. Wong and S. Mitragotri, *J. Controlled Release*, 2016, **238**, 176–185.
3 A. Salvati, A. S. Pitek, M. P. Monopoli, K. Prapainop, F. B. Bombelli, D. R. Hristov, P. M. Kelly, C. Aberg, E. Mahon and K. A. Dawson, *Nat. Nanotechnol.*, 2013, **8**, 137–143.
4 I. Lynch and K. A. Dawson, *Nano Today*, 2008, **3**, 40–47.
5 C. D. Walkey and W. C. W. Chan, *Chem. Soc. Rev.*, 2012, **41**, 2780–2799.
6 D. Docter, D. Westmeier, M. Markiewicz, S. Stolte, S. K. Knauer and R. H. Stauber, *Chem. Soc. Rev.*, 2015, **44**, 6094–6121.
7 S. Ritz, S. Schottler, N. Kotman, G. Baier, A. Musyanovych, J. Kuharev, K. Landfester, H. Schild, O. Jahn, S. Tenzer and V. Mailander, *Biomacromolecules*, 2015, **16**, 1311–1321.
8 H. Gao, Z. Yang, S. Zhang, S. Cao, S. Shen, Z. Pang and X. Jiang, *Sci. Rep.*, 2013, **3**, 2534.
9 L. Treuel, X. Jiang and G. U. Nienhaus, *J. R. Soc., Interface*, 2013, **10**, 20120939.
10 D. R. Hristov, L. Rocks, P. M. Kelly, S. S. Thomas, A. S. Pitek, P. Verderio, E. Mahon and K. A. Dawson, *Sci. Rep.*, 2015, **5**, 17040.
11 C. Pérez-Campaña, V. Gómez-Vallejo, M. Puigivila, A. Martín, T. Calvo-Fernández, S. E. Moya, R. F. Ziolo, T. Reese and J. Llop, *ACS Nano*, 2013, **7**, 3498–3505.
12 A. Silvestri, L. Polito, G. Bellani, V. Zambelli, R. P. Jumde, R. Psaro and C. Evangelisti, *J. Colloid Interface Sci.*, 2015, **439**, 28–33.
13 S. Nie, *Nanomedicine*, 2010, **5**, 523–528.
14 A. Li, H. P. Luehmann, G. Sun, S. Samarajeewa, J. Zou, S. Zhang, F. Zhang, M. J. Welch, Y. Liu and K. L. Wooley, *ACS Nano*, 2012, **6**, 8970–8982.
15 Y. Ji, Y. Wei, X. Liu, J. Wang, K. Ren and J. Ji, *J. Biomed. Mater. Res., Part A*, 2012, **100**, 1387–1397.
16 J. Muller, K. N. Bauer, D. Prozeller, J. Simon, V. Mailander, F. R. Wurm, S. Winzen and K. Landfester, *Biomaterials*, 2017, **115**, 1–8.
17 K. Rahme, L. Chen, R. G. Hobbs, M. A. Morris, C. O'Driscoll and J. D. Holmes, *RSC Adv.*, 2013, **3**, 6085–6094.
18 J. V. Jokerst, T. Lobovkina, R. N. Zare and S. S. Gambhir, *Nanomedicine*, 2011, **6**, 715–728.
19 E. Oh, J. B. Delehanty, K. E. Sapsford, K. Susumu, R. Goswami, J. B. Blanco-Canosa, P. E. Dawson, J. Granek, M. Shoff, Q. Zhang, P. L. Goering, A. Huston and I. L. Medintz, *ACS Nano*, 2011, **5**, 6434–6448.
20 S. J. H. Soenen, U. Himmelreich, N. Nuytten, T. R. Pisanic, A. Ferrari and M. De Cuyper, *Small*, 2010, **6**, 2136–2145.
21 Y. Tian, M. M. Martinez and D. Pappas, *Appl. Spectrosc.*, 2011, **65**, 115–124.
22 P. Schwille, F. J. Meyer-Almes and R. Rigler, *Biophys. J.*, 1997, **72**, 1878–1886.
23 S. Harutyunyan, A. Sedivy, G. Kohler, H. Kowalski and D. Blaas, *Methods Mol. Biol.*, 2015, **1221**, 83–100.
24 T. Liedl, S. Keller, F. C. Simmel, J. O. Rädler and W. J. Parak, *Small*, 2005, **1**, 997–1003.
25 N. Joshi, S. Basak, S. Kundu, G. De, A. Mukhopadhyay and K. Chattopadhyay, *Langmuir*, 2015, **31**, 1469–1478.
26 B. Sahoo, M. Goswami, S. Nag and S. Maiti, *Chem. Phys. Lett.*, 2007, **445**, 217–220.
27 G. U. Nienhaus, P. Maffre and K. Nienhaus, *Methods Enzymol.*, 2013, **519**, 115–137.
28 L. Shang and G. U. Nienhaus, *Acc. Chem. Res.*, 2017, **50**, 387–395.
29 C. Rocker, M. Potzl, F. Zhang, W. J. Parak and G. U. Nienhaus, *Nat. Nanotechnol.*, 2009, **4**, 577–580.
30 Y. Klapper, P. Maffre, L. Shang, K. N. Ekdahl, B. Nilsson, S. Hettler, M. Dries, D. Gerthsen and G. U. Nienhaus, *Nanoscale*, 2015, **7**, 9980–9984.
31 P. Maffre, S. Brandholt, K. Nienhaus, L. Shang, W. J. Parak and G. U. Nienhaus, *Beilstein J. Nanotechnol.*, 2014, **5**, 2036–2047.
32 B. Pelaz, P. del Pino, P. Maffre, R. Hartmann, M. Gallego, S. Rivera-Fernández, J. M. de la Fuente, G. U. Nienhaus and W. J. Parak, *ACS Nano*, 2015, **9**, 6996–7008.
33 P. Maffre, K. Nienhaus, F. Amin, W. J. Parak and G. U. Nienhaus, *Beilstein J. Nanotechnol.*, 2011, **2**, 374–383.
34 R. A. Murray, Y. Qiu, F. Chiodo, M. Marradi, S. Penades and S. E. Moya, *Small*, 2014, **10**, 2602–2610.

 This journal is © The Royal Society of Chemistry 2017

Published on 01 September 2017. Downloaded by CIC biomaGUNE on 10/10/2017 11:32:18.

35 F. Bertoli, D. Garry, M. P. Monopoli, A. Salvati and K. A. Dawson, *ACS Nano*, 2016, **10**, 10471–10479.
36 C. Åberg, J. A. Varela, L. W. Fitzpatrick and K. A. Dawson, *Sci. Rep.*, 2016, **6**, 34457.
37 E. Casals, T. Pfaller, A. Duschl, G. J. Oostingh and V. Puntes, *ACS Nano*, 2010, **4**, 3623–3632.
38 N. C. Reichardt, M. Martin-Lomas and S. Penades, *Chem. Commun.*, 2016, **52**, 13430–13439.
39 M. Moros, B. Hernáez, E. Garet, J. T. Dias, B. Sáez, V. Grazú, Á. González-Fernández, C. Alonso and J. M. de la Fuente, *ACS Nano*, 2012, **6**, 1565–1577.
40 L. E. van Vlerken, T. K. Vyas and M. M. Amiji, *Pharm. Res.*, 2007, **24**, 1405–1414.
41 L. Maus, O. Dick, H. Bading, J. P. Spatz and R. Fiammengo, *ACS Nano*, 2010, **4**, 6617–6628.
42 A. Silvestri, V. Zambelli, A. M. Ferretti, D. Salerno, G. Bellani and L. Polito, *Contrast Media Mol. Imaging*, 2016, **11**, 405–414.
43 T. L. Moore, L. Rodriguez-Lorenzo, V. Hirsch, S. Balog, D. Urban, C. Jud, B. Rothen-Rutishauser, M. Lattuada and A. Petri-Fink, *Chem. Soc. Rev.*, 2015, **44**, 6287–6305.
44 S. Tenzer, D. Docter, J. Kuharev, A. Musyanovych, V. Fetz, R. Hecht, F. Schlenk, D. Fischer, K. Kiouptsi, C. Reinhardt, K. Landfester, H. Schild, M. Maskos, S. K. Knauer and R. H. Stauber, *Nat. Nanotechnol.*, 2013, **8**, 772–781.
45 X. Jiang, S. Weise, M. Hafner, C. Röcker, F. Zhang, W. J. Parak and G. U. Nienhaus, *J. R. Soc., Interface*, 2010, **7**, S5–S13.
46 P. Sandin, L. W. Fitzpatrick, J. C. Simpson and K. A. Dawson, *ACS Nano*, 2012, **6**, 1513–1521.
47 J. A. Kim, C. Aberg, A. Salvati and K. A. Dawson, *Nat. Nanotechnol.*, 2011, **7**, 62–68.
48 R. A. Petros and J. M. DeSimone, *Nat. Rev. Drug Discovery*, 2010, **9**, 615–627.
49 N. Altan-Bonnet and G. Altan-Bonnet, *Curr. Protoc. Cell Biol.*, 2009, Chapter 4, Unit 4.24, pp. 1–14.